Reconfigurable ultraviolet and high-energy-visible dielectric metamaterials

Behrad Gholipour[1, 2, 3*], Davide Piccinotti[1*], Artemios Karvounis[1], Kevin F. MacDonald[1], and Nikolay I. Zheludev[1, 4]

[1] Optoelectronics Research Centre and Centre for Photonic Metamaterials, University of Southampton, Highfield, Southampton, SO15 4JB, UK

[2] Department of Chemistry, University of Southampton, Highfield, Southampton, SO15 4JB, UK

[3] Department of Electrical and Computer Engineering, University of Alberta, Edmonton, Canada

[4] Centre for Disruptive Photonic Technologies, School of Physical and Mathematical Sciences and The Photonics Institute, Nanyang Technological University, 637371, Singapore

Photonic materials with tuneable and switchable ultraviolet (UV) to high-energy-visible (HEV) optical properties would benefit applications in sensing, high-density optical memory, beam-steering, adaptive optics and light modulation. Here, for the first time, we demonstrate a non-volatile switchable dielectric metamaterial operating in the UV-HEV spectral range. Nano-grating metamaterials in a layered composite of low-loss ZnS/SiO_2 and the chalcogenide phase-change medium germanium antimony telluride ($Ge_2Sb_2Te_5$) exhibit reflection resonances at UV-HEV wavelengths that are substantially modified by light-induced (amorphous-crystalline) phase transitions in the chalcogenide layer. Despite the presence of the lossy GST, resonance quality factors up to Q~15 are ensured by the transparency (low losses) of ZnS/SiO_2 in the UV-HEV spectral range and values of Q increase as the refractive index of $Ge_2Sb_2Te_5$ decreases, upon crystallization. Notably however, this switching leaves resonance spectral positions unchanged.

KEYWORDS: *metamaterials, chalcogenides, ultraviolet, optical switching, phase change, all-dielectric metamaterials, reconfigurable metasurfaces*

Photonic metamaterials - artificial electromagnetic media structured on the subwavelength scale - are now a well-established enabling technology paradigm for engineering electromagnetic space and (actively) controlling the propagation of light and its interaction with matter[1-3]. An extensive range of enhanced and unusual optical properties, including dynamically tuneable/switchable and nonlinear functionalities, have been demonstrated at technologically important near-infrared and visible frequencies in metamaterials and metasurfaces comprised of nanostructured plasmonic metals (very typically gold), high-index dielectrics (often silicon[4-8], but also GaAs[9], germanium[10], perovskites[11] and chalcogenides[12, 13]) and metal/dielectric composites.

However, while the ultraviolet (UV) and short-wavelength, high-energy visible (HEV) spectral range (200-500 nm) is of considerable interest and importance to a variety of applications in the physical, environmental, manufacturing and bio-sciences[14-22], it is less often the focus of attention in metamaterials research than the longer-wavelength visible / near-infrared domain. A significant factor in this, aside from dimensional requirements/constraints on nanofabrication for shorter wavelengths, is the fact that the aforementioned archetypal material platforms (gold and silicon) are unsuitable in the UV-HEV band. Alternative materials are though available: silver and aluminium for example are good plasmonic metals at short UV/HEV wavelengths beyond the reach of gold[23] (although they are subject to atmospheric degradation, i.e. oxidation/tarnishing); and materials such as diamond, alumina and zinc sulphide are transparent, relatively high-index dielectrics in this range (i.e. of sufficiently high index, relative to air as the assumed incident medium, to support Mie-type dielectric nano-cavity resonances). However, none of these are intrinsically 'active' media able to provide dynamic, reversible, thermally/electrically/optically-controlled tuning and switching functionalities. Here, we realize the first optically reconfigurable

UV/HEV dielectric metasurface by hybridizing a transparent passive dielectric nanostructure with a chalcogenide that acts in this spectral range as a *low*-index phase-change medium. Chalcogenide semiconductor alloys are noted for presenting an assortment of compositionally variable properties, from infrared transparency and high optical nonlinearity to photorefractivity and non-volatile phase switching between amorphous and crystalline states with often markedly different optoelectronic properties[24-29]. As such they have been employed as functional (i.e. phase-change) dielectrics in near- to mid-IR hybrid plasmonic (noble metal) and all-dielectric metamaterials for applications including signal intensity and polarization modulation, beam steering, and multispectral imaging[12, 13, 25, 30-39].

While generally known for their high refractive indices at infrared frequencies, it is less widely appreciated that chalcogenides are characteristically low-index (albeit lossy) dielectric and plasmonic media at shorter wavelengths (Figure S1) [35, 40-42]. Indeed, in the UV/HEV spectral range, they can have lower refractive indices than most oxides, nitrides and perovskites. Here we harness this low refractive index along with their phase-switchable character to realise the first optically reconfigurable UV/HEV dielectric metamaterials, in which the functional chalcogenide is hybridised with a transparent, high-index dielectric nanostructure supporting the resonant mode. Laser-induced crystallization of the amorphous chalcogenide decreases its refractive index and is found to increase metamaterial resonance quality *without* spectrally shifting the resonance and *in spite of* the fact that the crystalline phase has a higher extinction coefficient.

Results and Discussion. The present study employs germanium antimony telluride (Ge_2:Sb_2:Te_5 or GST) – a chalcogenide alloy widely used in rewritable optical (DVD/Blu-ray) and electronic data storage (PCRAM) technologies with a refractive index as low as 1.07 at 245 nm in the crystalline phase, and an amorphous composite of zinc sulphide and silica (ZnS/SiO_2 in a 1:9 at% ratio) – a transparent dielectric with an essentially non-dispersive

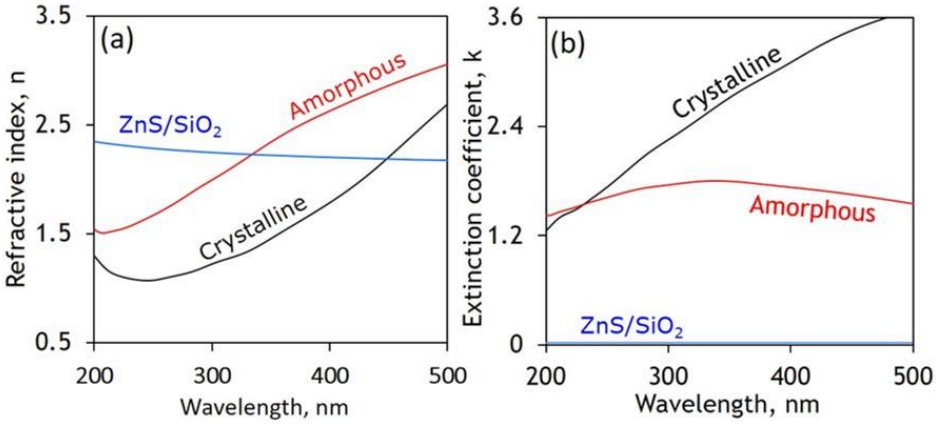

Figure 1. UV-HEV optical properties of GST and ZnS/SiO_2. Spectral dispersion [from variable angle ellipsometric measurements] of (a) the refractive index *n* and (b) corresponding extinction coefficient *k* for germanium antimony telluride [GST] in amorphous and crystalline phases [as labelled] and for ZnS/SiO_2.

UV-VIS index of ~2.4. As such, ZnS/SiO_2 has a higher index than amorphous GST for wavelengths up to 338 nm and a higher index than crystalline GST up to 475 nm (Figure 1a). Both phases of GST have substantially higher extinction coefficients relative to ZnS/SiO_2, with that of the crystalline phase being generally somewhat higher than that of the amorphous phase (Figure 1b).

Metamaterial structures were fabricated in a tri-layer of 70 nm GST between two 70 nm layers of ZnS/SiO_2 deposited on optically flat silica substrates by RF sputtering. The metamaterial consists of sub-wavelength period (i.e. non-diffractive) grating patterns, with a fixed linewidth W~50 nm and periods P ranging from 300 to 400 nm and reconfigured using femtosecond optical pulses (see Methods, Figure 2). The reflectivity of the unstructured ZnS/SiO_2–GST–ZnS/SiO_2 tri-layer is higher when the GST layer is in its crystalline state than when it is in the amorphous state, and in both cases, decreases monotonically with increasing wavelength over the UV to high energy visible spectral range, as shown in Figure

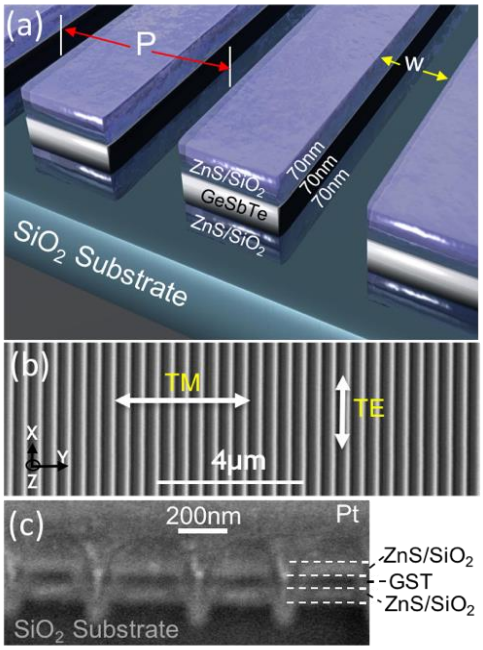

Figure 2. Reconfigurable UV-HEV all-dielectric metamaterials. (a) Artistic cut-away section of nano-grating metamaterial structure fabricated in a tri-layer of 70 nm GST between two layers [70 nm each] of ZnS/SiO_2. (b) Scanning electron microscope image of a section of such a metamaterial [dark areas being nano-grating lines milled through the tri-layer to the underlying quartz substrate]. (c) Cross-sectional scanning electron microscope image showing the layers of the metamaterial.

3a, b. The nano-grating metamaterial structures present reflection resonances for incident light polarised parallel to the grating lines (along the *x* direction defined in Figure 2b; or the TE orientation of the grating), which are based upon the interaction between thin film interference and grating modes[43, 44]. These occur at spectral positions dependent upon the period *P* but not upon the phase state of the GST layer (Figure 3a-d), as may be expected on the basis of prior works relating to the switching and tuning of metamaterial resonances (e.g. via a near-field refractive index change or nano-mechanical reconfiguration[12, 13, 45]). Here, the amorphous-to-crystalline transition in the GST layer brings about an increase in the quality-factor of the resonances (defined here as $Q = \lambda_R/\Delta\lambda$, where λ_R is the reflection

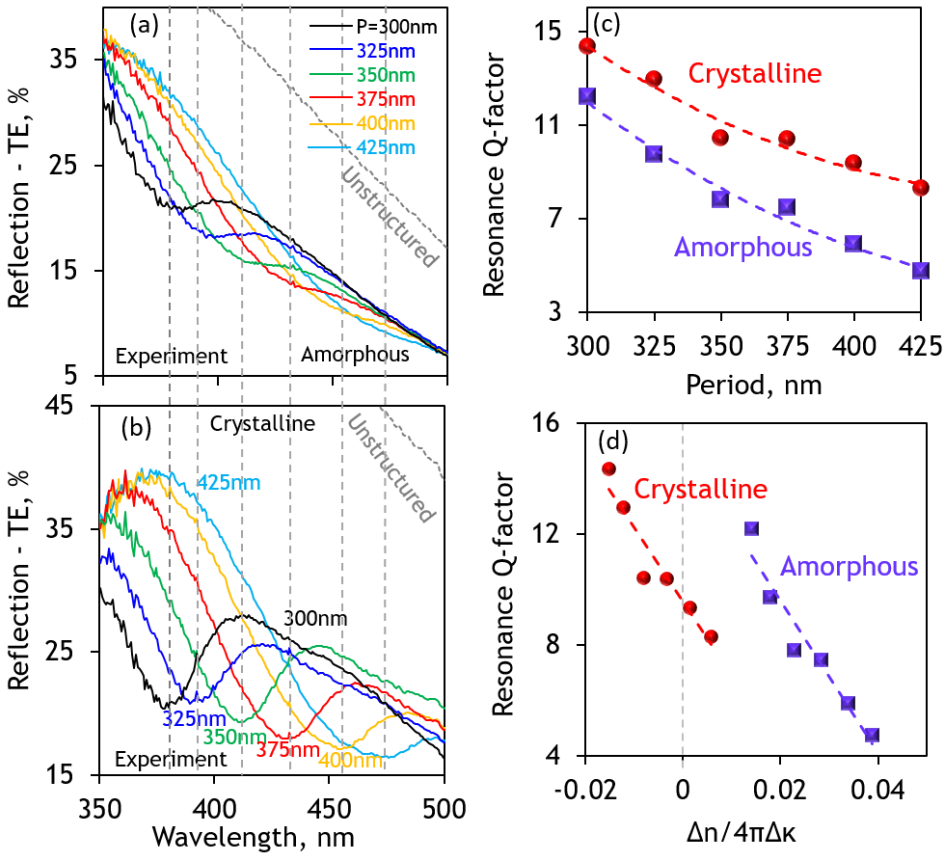

Figure 3. Optical properties of ZnS/SiO₂–GST metamaterials. (a, b) Measured spectral dispersion of ZnS/SiO₂–GST–ZnS/SiO₂ nano-grating metamaterial TE reflection for a selection of grating periods *P* [as labelled], for the amorphous (a) and polycrystalline (b) states of the GST layer, overlaid with corresponding spectra for the unstructured tri-layer [dotted lines]. (c, d) Measured resonance quality factor *Q* as a function of (c) metamaterial period *P*, (d) index contrast figure of merit.

resonance wavelength and $\Delta\lambda$ is the half-maximum linewidth), by a factor of up to 1.7, without a change in spectral position (Figure 3c). For both phase states of GST, *Q* decreases with increasing metamaterial period *P*, which is to say with increasing resonance wavelength λ_R. This is as a result of the changing balance between the refractive indices of GST (in either phase) and that of ZnS/SiO₂: *Q* is largest for the shortest period gratings (shortest, UV resonance wavelengths) with GST in the crystalline phase, where $\Delta n = n_{GST} - n_{ZnS/Sio_2}$

assumes its largest negative value; and smallest for the largest period gratings (longest, HEV resonance wavelengths) with GST in the amorphous state, where Δn takes its largest positive value (Figure 3d).

That the balance between the refractive indices of GST and ZnS/SiO_2 is the key determinant of metamaterial resonance quality is further illustrated by the fact that *Q* increases with GST crystallisation, i.e. with decreasing GST index (increasing index contrast Δn), in spite of the associated increase in GST extinction coefficient *k* (see Figure 1b). This is because the chalcogenide's extinction coefficient in both phase states is much larger than that of the ZnS/SiO_2. That said, values of *k* for the crystalline phase are higher and increase more rapidly with wavelength than for the amorphous phase, and this does play into the dispersion of *Q*.

As a figure of merit (FOM) describing the ability of a dielectric resonator to support low loss propagating waves within its volume we may take the dissipation length of a transverse electromagnetic wave $\mathrm{d} = \lambda_0/4\pi\kappa$ in units of wavelength $\lambda = \lambda_0/\mathrm{n}$, where *n* and *k* are respectively the medium's refractive index and extinction coefficient and λ_0 is the free space wavelength: $\mathrm{FOM} = \mathrm{n}/4\pi\kappa$. In the present case, where there are two materials – GST and ZnS/SiO_2, resonance quality depends on the contrast Δn, Δk between refractive indices and extinction coefficients of (or in other words the impedance mismatch between) the two media: the same proportionality is seen (Figure 3d) for both phase states between *Q* and the quantity $\Delta n/_{4\pi\Delta k}$.

The observed change in metamaterial resonance quality *Q* without an associated change in resonance wavelength λ_R, is made possible by the fact that the structural transition in the GST layer predominantly affects the distribution and confinement of field (the 'leakiness' of the mode) in the overlying ZnS/SiO_2 layer. Figure 4 show results of a 2D finite-difference-time-domain (FDTD) model, which employs ellipsometrically measured values for the complex permittivity of GST and ZnS/SiO_2 as presented in Figure 1.

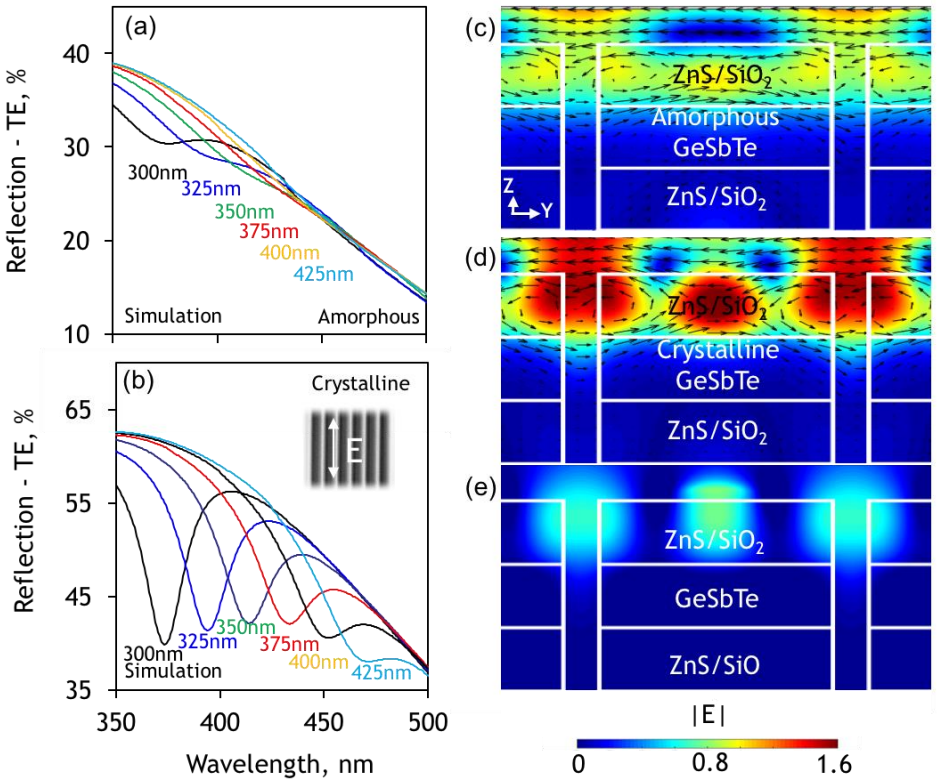

Figure 4. Numerically simulated optical response of hybrid chalcogenide phase-change medium / transparent dielectric metamaterials. Spectral dispersion of ZnS/SiO_2–GST–ZnS/SiO_2 nano-grating metamaterial TE reflection for a selection of grating periods *P* [as labelled], for the amorphous (a) and polycrystalline (b) states of the GST layer. (c, d) Distributions of the normalized electric field, |*E*| in the *yz*-plane for a nano-grating of period *P* = 300 nm at its reflection resonance wavelength λ_R = 375nm, overlaid with arrows denoting the direction and magnitude of magnetic field, for the amorphous (c) and polycrystalline (d) states of the GST layer. (e) Corresponding change in the strength and spatial distribution of field between the two phase states of the GST layer, evaluated as the difference between panels (c) and (d).

There is very good qualitative and quantitative agreement between experimentally measured (Figure 3a, b) and numerically simulated (Figure 4a, b) reflection spectra for the tri-layer

metamaterials, for both the amorphous and crystalline states of the GST layer. Minor discrepancies are attributed to manufacturing imperfections, i.e. deviations from the ideal model geometry such as slight over-milling of grating lines into the substrate, and the tapered/rounded cross-sectional profile of milled lines; and to contamination/stoichiometric change in the ZnS/SiO_2 and/or GST layers during FIB milling, which may slightly modify refractive index.

These simulations show that for any given metamaterial period, the decrease of GST layer refractive index associated with its crystallization enhances field confinement (local field strength) in the overlying ZnS/SiO_2 layer (Figure 4c, d). There is consequently an increase in resonance quality Q without a change in resonance wavelength λ_R and despite the higher extinction coefficient of crystalline (as compared to amorphous) GST, because there is minimal penetration of fields into the GST layer in either phase state. Interestingly, the differential field map shown in Figure 4e indicates that local fields are enhanced upon GST crystallization both within the ZnS/SiO_2 and in the gaps between the nano-grating lines. This is distinctly different from the switching behaviour usually seen in either plasmonic or all-dielectric metamaterials, where substantive changes in field strength occur either within the gaps of a plasmonic nanostructure or within the volume of high-index dielectric resonator elements, not both.

Conclusion and Perspectives. We have demonstrated an approach that enables for the first time non-volatile switching of dielectric metamaterial optical properties in the UV/HEV spectral range: By combining a relatively low refractive index chalcogenide phase-change medium with a transparent high-index dielectric, we realize a hybrid all-dielectric nanostructure in which optically-induced (amorphous-crystalline) phase switching of the chalcogenide component changes the quality of metamaterial resonances based upon optical

field confinement in the dielectric *without* affecting their spectral position. Moreover, counterintuitively, metamaterial resonance quality increases as the extinction coefficient of the chalcogenide increases.

In the present case, we utilize $Ge_2Sb_2Te_5$ (GST) as the functional phase-change medium and ZnS/SiO_2 as a transparent dielectric (of sufficiently high refractive index relative to the incident medium as to support dielectric cavity resonances when nanostructured) – achieving, for a simple nano-grating metamaterial design - a maximum reflection resonance quality factor Q~15 at a wavelength of 380 nm and a change in Q of at least 20% with GST phase switching. The concept though may be applied for the introduction of non-volatile switching (memory) functionality to a variety of otherwise passive UV/HEV material platforms for all-dielectric metamaterials: Higher quality factors may be achieved through the use of higher-index dielectrics and/or lower-index chalcogenides – there are, for example, BiTe and SbTe alloys which offer sub-unitary refractive indices in the UV-visible spectral range[40, 46], albeit with reduced switching contrast between phase states as compared to GST. The mechanism is furthermore scalable to other spectral bands, presenting possibilities for non-volatile switching in a wide variety of meta-surface 'flat-optic' applications.

Methods. *Metadevice Fabrication.* Metamaterial structures were fabricated in a tri-layer of 70 nm GST between two 70 nm layers of ZnS/SiO_2 deposited on optically flat silica substrates by RF sputtering (Kurt J. Lesker Nano 38) from $Ge_2Sb_2Te_5$ and $ZnS:SiO_2$ (1:9) targets. A base pressure of 5×10^{-7} mbar was achieved prior to deposition and high-purity argon was used as the sputtering gas. The substrate was held within 10K of room temperature on a rotating platen 150 mm from the target so as to produce low-stress amorphous films. The role of the bottom layer is not optical but mechanical: When encapsulating a phase-change thin film, it is good practice to deposit the same material on either side of the phase-change

layer to avoid the application of uneven stress, which can compromise the long-term stability of devices. Sub-wavelength period (i.e. non-diffractive) grating patterns, with a fixed linewidth W~50 nm and periods P ranging from 300 to 400 nm, each covering an area of approximately 20 μm × 20 μm, were etched through the ZnS/SiO_2–GST–ZnS/SiO_2 tri-layer by focused ion beam (FIB) milling (FEI Helios NanoLab 600), as illustrated in Figure 2).

Optical Switching. The amorphous-to-crystalline transition in chalcogenides is an annealing process that can be initiated uniformly over an entire sample by increasing the ambient temperature to a point above the material's glass-transition point T_g (~160°C for GST) but below its melting point T_m (~600°C)[47], or by locally applying electrical current or laser-induced heating, as in the present study: transitions in the GST layer from the as-deposited amorphous state to the crystalline state were excited using trains of fifty 85 fs, 140 $mJ.cm^{-2}$ laser pulses at a wavelength of 730 nm and a repetition rate of 1 MHz.

Experimental Metadevice Characterization. Normal-incidence reflection characteristics of the unstructured tri-layer and the nano-grating metamaterials were quantified using a microspectrophotometer (CRAIC QDI2010) with a sampling domain size of 10 μm × 10 μm and numerical aperture of 0.28.

Numerical Simulations. Lumerical FDTD Solutions was used to develop a 2D finite-difference-time-domain (FDTD) model, which employs ellipsometrically measured values for the complex permittivity of GST and ZnS/SiO_2 as presented in Figure 1. It assumes a lossless non-dispersive refractive index of 1.46 for the semi-infinite silica substrate; normally-incident narrowband plane wave illumination; and by virtue of periodic boundary conditions, nano-grating patterns of infinite extent in the *x*-*y* plane.

Associated Content. The data from this paper is available from the University of Southampton ePrints research repository.

Author information.

Corresponding author: E-mail: bgholipo@ualberta.ca

B.G and D.P contributed equally to this work.

Notes

The authors declare no competing financial interest.

Acknowledgements

This work was supported by the UK Engineering and Physical Sciences Research Council [grants EP/M009122/1 and EP/N00762X/1] and the Singapore Ministry of Education [grant MOE2016-T3-1-006].

References

1. Zheludev, N. I.; Kivshar, Y. S. *Nat. Mater*. **2012,** 11, (11), 917-24.
2. Urbas, A. M.; Jacob, Z.; Dal Negro, L.; Engheta, N.; Boardman, A. D.; Egan, P.; Khanikaev, A. B.; Menon, V.; Ferrera, M.; Kinsey, N.; DeVault, C.; Kim, J.; Shalaev, V.; Boltasseva, A.; Valentine, J.; Pfeiffer, C.; Grbic, A.; Narimanov, E.; Zhu, L. X.; Fan, S. H.; Alu, A.; Poutrina, E.; Litchinitser, N. M.; Noginov, M. A.; MacDonald, K. F.; Plum, E.; Liu, X. Y.; Nealey, P. F.; Kagan, C. R.; Murray, C. B.; Pawlak, D. A.; Smolyaninov, II; Smolyaninova, V. N.; Chanda, D. *J. Opt.* **2016,** 18, (9), 53.
3. Genevet, P.; Capasso, F.; Aieta, F.; Khorasaninejad, M.; Devlin, R. *Optica* **2017,** 4, (1), 139.
4. Zhang, J.; MacDonald, K. F.; Zheludev, N. I. *Opt. Express* **2013,** 21, 26721-26728.

5. Wu, C.; Arju, N.; Kelp, G.; Fan, J. A.; Dominguez, J.; Gonzales, E.; Tutuc, E.; Brener, I.; Shvets, G. *Nat. Commun.* **2014,** 5, 3892.
6. Moitra, P.; Slovick, B. A.; Gang Yu, Z.; Krishnamurthy, S.; Valentine, J. *Appl. Phys. Lett.* **2014,** 104, (17), 171102.
7. West, P. R.; Stewart, J. L.; Kildishev, A. V.; Shalaev, V. M.; Shkunov, V. V.; Strohkendl, F.; Zakharenkov, Y. A.; Dodds, R. K.; Byren, R. *Opt. Express* **2014,** 22, (21), 26212.
8. Decker, M.; Staude, I.; Falkner, M.; Dominguez, J.; Neshev, D.; Brener, I.; Pertsch, T.; Kivshar, Y. *Adv. Opt. Mater.* **2015,** 3, (6), 813 - 820.
9. Löchner, F. J. F.; Fedotova, A. N.; Liu, S.; Keeler, G. A.; Peake, G. M.; Saravi, S.; Shcherbakov, M. R.; Burger, S.; Fedyanin, A. A.; Brener, I.; Pertsch, T.; Setzpfandt, F.; Staude, I. *ACS Photonics* **2018,** 5, (5), 1786-1793.
10. Li, Y.; Clady, R.; Park, J.; Thombare, S. V.; Schmidt, T. W.; Brongersma, M. L.; McIntyre, P. C. *Nano Lett.* **2014,** 14, (6), 3427-31.
11. Gholipour, B.; Adamo, G.; Cortecchia, D.; Krishnamoorthy, H. N. S.; Birowosuto, M. D.; Zheludev, N. I.; Soci, C. *Adv. Mater.* **2017,** 29, (9), 1604268.
12. Wang, Q.; Rogers, E. T. F.; Gholipour, B.; Wang, C. M.; Yuan, G. H.; Teng, J. H.; Zheludev, N. I. *Nat. Photonics* **2016,** 10, (1), 60-U75.
13. Karvounis, A.; Gholipour, B.; MacDonald, K. F.; Zheludev, N. I. *Appl. Phys. Lett.* **2016,** 109, (5), 051103.
14. Tabataba-Vakili, F.; Roland, I.; Tran, T.-M.; Checoury, X.; El Kurdi, M.; Sauvage, S.; Brimont, C.; Guillet, T.; Rennesson, S.; Duboz, J.-Y.; Semond, F.; Gayral, B.; Boucaud, P. *Appl. Phys. Lett.* **2017,** 111, (13), 131103.

15. Wunderer, T.; Chua, C. L.; Northrup, J. E.; Yang, Z.; Johnson, N. M.; Kneissl, M.; Garrett, G. A.; Shen, H.; Wraback, M.; Moody, B.; Craft, H. S.; Schlesser, R.; Dalmau, R. F.; Sitar, Z. *physica status solidi (c)* **2012,** 9, (3-4), 822-825.
16. Stegmaier, M.; Ebert, J.; Meckbach, J. M.; Ilin, K.; Siegel, M.; Pernice, W. H. P. *Appl. Phys. Lett.* **2014,** 104, (9), 091108.
17. Soltani, M.; Soref, R.; Palacios, T.; Englund, D. *Optics Express* **2016,** 24, (22), 25415.
18. Razeghi, M.; Rogalski, A. *Journal of Applied Physics* **1996,** 79, (10), 7433-7473.
19. Li, K. H.; Liu, X.; Wang, Q.; Zhao, S.; Mi, Z. *Nature Nanotechnology* **2015,** 10, (2), 140-144.
20. Kneissl, M.; Kolbe, T.; Chua, C.; Kueller, V.; Lobo, N.; Stellmach, J.; Knauer, A.; Rodriguez, H.; Einfeldt, S.; Yang, Z.; Johnson, N. M.; Weyers, M. *Semiconductor Science and Technology* **2010,** 26, (1), 014036.
21. Asif Khan, M.; Shatalov, M.; Maruska, H. P.; Wang, H. M.; Kuokstis, E. *Japanese Journal of Applied Physics* **2005,** 44, (10), 7191-7206.
22. Argyropoulos, C.; Monticone, F.; D'Aguanno, G.; Alù, A. *Appl. Phys. Lett.* **2013,** 103, (14), 143113.
23. West, P. R.; Ishii, S.; Naik, G. V.; Emani, N. K.; Shalaev, V. M.; Boltasseva, A. *Laser Photonics Rev.* **2010,** 4, (6), 795-808.
24. Eggleton, B. J.; Luther-Davies, B.; Richardson, K. *Nat. Photon* **2011,** 5, (3), 141-148.
25. Wuttig, M.; Bhaskaran, H.; Taubner, T. *Nat. Photon* **2017,** 11, (8), 465-476.
26. Gholipour, B.; Bastock, P.; Craig, C.; Khan, K.; Hewak, D.; Soci, C. *Adv. Opt. Mater* **2015,** 3, (5), 634-634.
27. Borisenko, K. B.; Shanmugam, J.; Williams, B. A. O.; Ewart, P.; Gholipour, B.; Hewak, D. W.; Hussain, R.; Jávorfi, T.; Siligardi, G.; Kirkland, A. I. *Scientific Reports* **2015,** 5, 8770.

28. Huang, C. C.; Gholipour, B.; Ou, J. Y.; Knight, K.; Hewak, D. W. *Electronics Letters* **2011,** 47, (4), 288.

29. Hewak, D.; Gholipour, B. *Science* **2012,** 336, (6088), 1515-1516.

30. Gholipour, B.; Zhang, J.; MacDonald, K. F.; Hewak, D. W.; Zheludev, N. I. *Adv. Mater.* **2013,** 25, (22), 3050-3054.

31. Chen, Y. G.; Kao, T. S.; Ng, B.; Li, X.; Luo, X. G.; Luk'yanchuk, B.; Maier, S. A.; Hong, M. H. *Opt. Express* **2013,** 21, (11), 13691-13698.

32. Tittl, A.; Michel, A.-K. U.; Schaeferling, M.; Yin, X.; Gholipour, B.; Cui, L.; Wuttig, M.; Taubner, T.; Neubrech, F.; Giessen, H. *Adv. Mater.* **2015,** 27, (31), 4597-4603.

33. Rude, M.; Pello, J.; Simpson, R. E.; Osmond, J.; Roelkens, G.; van der Tol, J. J. G. M.; Pruneri, V. *Appl. Phys. Lett.* **2013,** 103, (14), 141119.

34. Krishnamoorthy, H. N. S.; Gholipour, B.; Zheludev, N. I.; Soci, C. *Adv. Opt. Mater.* **2018,** 6, (19), 1800332.

35. Gholipour, B.; Karvounis, A.; Yin, J.; Soci, C.; MacDonald, K. F.; Zheludev, N. I. *NPG Asia Mater.* **2018,** 10, 533-539.

36. Yin, X.; Steinle, T.; Huang, L.; Taubner, T.; Wuttig, M.; Zentgraf, T.; Giessen, H. *Light: Science & Applications* **2017,** 6, (7), e17016.

37. Chu, C. H.; Tseng, M. L.; Chen, J.; Wu, P. C.; Chen, Y.-H.; Wang, H.-C.; Chen, T.-Y.; Hsieh, W. T.; Wu, H. J.; Sun, G.; Tsai, D. P. *Laser & Photonics Reviews* **2016,** 10, (6), 986-994.

38. Ahmadivand, A.; Gerislioglu, B.; Sinha, R.; Karabiyik, M.; Pala, N. *Scientific Reports* **2017,** 7, (1).

39. Ahmadivand, A.; Gerislioglu, B.; Pala, N. *Jour. Phys. Chem C* **2017,** 121, (36), 19966-19974.

40. Piccinotti, D.; Gholipour, B.; Yao, J.; Macdonald, K. F.; Hayden, B. E.; Zheludev, N. I. *Optics Express* **2018,** 26, (16), 20861.
41. Yin, J.; Krishnamoorthy, H. N. S.; Adamo, G.; Dubrovkin, A. M.; Chong, Y.; Zheludev, N. I.; Soci, C. *NPG Asia Materials* **2017,** 9, (8), e425.
42. Toudert, J.; Serna, R. *Opt. Mater. Express* **2017,** 7, (7), 2299-2325.
43. D'Aguanno, G.; de Ceglia, D.; Mattiucci, N.; Bloemer, M. J. *Optics Letters* **2011,** 36, (11), 1984.
44. Fan, S.; Suh, W.; Joannopoulos, J. D. *Journal of the Optical Society of America A* **2003,** 20, (3), 569.
45. Zheludev, N. I.; Plum, E. *Nat. Nanotechnol.* **2016,** 11, (1), 16-22.
46. Piccinotti, D.; Gholipour, B.; Yao, J.; Macdonald, K. F.; Hayden, B. E.; Zheludev, N. I., Extraordinary Properties of Epsilon-Near-Zero and Low-Index Chalcogenide Metamaterials. In *Conference on Lasers and Electro-Optics*, OSA: 2018.
47. Orava, J.; Greer, A. L.; Gholipour, B.; Hewak, D. W.; Smith, C. E.; Loke, D.; Lee, T. H.; Wang, W. J.; Shi, L. P.; Zhao, R.; Yeo, Y. C.; Chong, T. C.; Elliott, S. R. *Nat. Mater.* **2012,** 11, (4), 279-283.